Inorganic Chemistry

Article

pubs.acs.org/IC

Synthesis and Disordered Crystal Structure of $Al_3O_{3.5}C_{0.5}$

Toru Asaka,[†] Ryosuke Kotani,[†] Tatsunari Kudo,[†] Hideto Yoshida,[‡] and Koichiro Fukuda*,[†]

[†]Department of Materials Science and Engineering, Nagoya Institute of Technology, Nagoya 466-8555, Japan

[‡]Department of Earth and Planetary Science, Graduate School of Science, The University of Tokyo, Tokyo 113-0033, Japan

Supporting Information

ABSTRACT: The crystal structure of $Al_3O_{3.5}C_{0.5}$ ($Z = 3$) has been characterized by X-ray powder diffraction (XRPD), transmission electron microscopy, and electron probe microanalysis. The title compound is trigonal with space group $R\bar{3}m$ (centrosymmetric) and hexagonal unit-cell dimensions a = 0.29588(1) nm, c = 2.84080(7) nm, and V = 0.21538(1) nm^3. The initial structural model was determined by the charge-flipping method and subsequently refined by the Rietveld method. The final structural model showed the positional disordering of one of the two types of Al sites. The maximum-entropy method-based pattern fitting (MPF) method was used to confirm the validity of the split-atom model, in which conventional structure bias caused by assuming intensity partitioning was minimized. The reliability indices calculated from the MPF were R_{wp} = 4.03%, S (= R_{wp}/R_e) = 1.17, R_p = 3.08%, R_B = 0.82%, and R_F = 0.72%. The crystal was composed of antiphase domains, suggesting the occurrence of the high-low phase transition during the cooling process. The transition would be accompanied by the loss of unit-lattice translation, and hence the disordered structural model determined by XRPD might be of the average structure of the low-temperature phase.

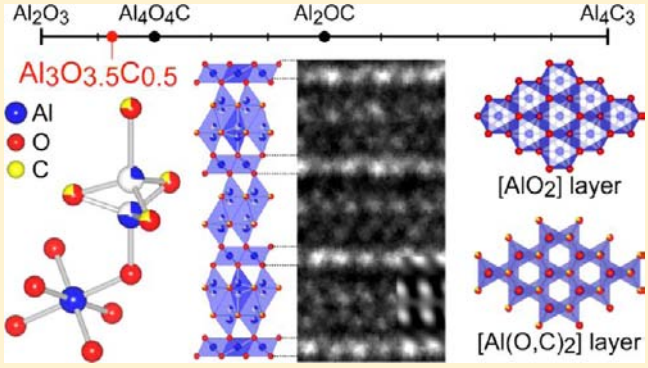

INTRODUCTION

In the system Al−O−C, there are four types of binary and ternary compounds established so far; they are Al_2O_3, Al_4C_3, Al_4O_4C, and Al_2OC.[1] The chemical compositions of the latter two compounds necessarily lie on the tie line Al_2O_3−Al_4C_3. In this binary system, Sitnikov et al. have reported a new aluminum oxycarbide, $Al_3O_{3.5}C_{0.5}$ ($2Al_2O_3{\cdot}Al_2OC$ or Al_6O_7C in the original report).[2] However, we have insufficient characterization data for this material, partly because its crystal structure has not yet been clarified. In the crystal structure of α-Al_2O_3 the oxygen atoms are arranged in approximately hexagonal close packing.[3] Between the two oxygen layers there are positions for Al atoms such that each one is surrounded by six O atoms arranged octahedrally. Only two-thirds of the available positions are filled, with the remaining one-third of these being vacant. With Al_4C_3, the crystal structure can be described in terms of a three-dimensional network of [AlC_4] tetrahedra which are associated by sharing corners and edges.[4] The average Al−C distance of [AlC_4] tetrahedra is 0.206 nm for Al_4C_3. With [AlO_4] tetrahedra, the ionic radii of Al^{3+} in the 4-fold coordination [$r(Al^{3+}(4))$ = 0.039 nm and $r(O^{2-}(4))$ = 0.138 nm][5] predicts the interatomic distance of 0.177 nm. Thus, the average interatomic distances are generally longer for [AlC_4] than for [AlO_4].

Recent advances in the field of crystal-structure analysis from X-ray powder diffraction (XRPD) data have enabled us to investigate unknown structures as well as complex structures, including positional disordering of atoms. To begin with, initial structural models are required, which may be determined by, for example, powder charge-flipping method.[6,7] The structural parameters are subsequently refined using the Rietveld method.[8] A combined use of the Rietveld method, the maximum-entropy method (MEM),[9] and the MEM-based pattern fitting (MPF) method[10] has enabled us to disclose new structural details. MEM is capable of estimating structure factors of unobserved reflections and improving those of overlapped reflections, which give MEM advantages over the classical Fourier method. However, the Rietveld method and MEM have a drawback in determining the electron-density distributions (EDD) because the observed structure factors, F_o(Rietveld), are biased toward the structural model assuming intensity partitioning. On the other hand, the MPF method can minimize the structural bias. Thus, the MEM and MPF analyses are alternately repeated (REMEDY cycle) until the reliability indices reach minima. Crystal structures can be seen clearly from EDD determined by MPF. Nevertheless, the X-ray diffraction methods only determine the time- and space-averaged distribution of atoms. Transmission electron microscopy (TEM) is an effective technique for the local structure investigations. These two types of methods are complementary, and both are indispensible tools for identifying unknown phases.

Intracrystalline microstructures in crystals are often induced by phase transitions that occur during the cooling process. When the low temperature phase is a subgroup of the high

Received: December 5, 2012
Published: February 14, 2013

   dx.doi.org/10.1021/ic302674g | *Inorg. Chem.* 2013, 52, 2648−2653

temperature phase, two fundamentally different types of microstructures result: antiphase domains (APDs) and twin domains. The APDs arise from transitions in which the point group remains the same but the number of lattice points per unit volume is reduced.[11] The displacement vector relating the domains is the vector from the origin to the lost lattice point. The APD boundaries are made visible in TEM because of a change in the phase of the electron beam as it crosses the boundary. The formation of APDs is usually accompanied by the appearance of extra reflections in the electron diffraction pattern.

In the present study, we have structurally characterized $Al_3O_{3.5}C_{0.5}$ in the Al_2O_3–Al_4C_3 system. The crystal structure has been expressed by the split-atom model, in which one of the two types of Al sites is positionally disordered. The crystal is probably composed of APDs with ordered crystal structure.

EXPERIMENTAL SECTION

Materials. The reagent-grade chemicals of Al (99.9%, KCL Co., Ltd., Saitama, Japan), Al_2O_3 (99%, Kishida Chemical Co., Ltd., Osaka, Japan), and Al_4C_3 (98%, Mitsuwa Chemical Co., Ltd., Kanagawa, Japan) were mixed in molar ratios of [Al:Al_2O_3:Al_4C_3] = [3:5:2], corresponding to [Al:O:C] = [7:5:2] (Figure S1, see Supporting Information). The well-mixed chemicals were pressed into pellets (φ25 mm × 10 mm), loaded into an open carbon crucible, heated in a carbon resistance furnace (FVHP-R-1, Fuji Dempa Kogyo Co. Ltd., Osaka, Japan) at 2223 K for 1 h in inert gas atmosphere of Ar, followed by cooling to ambient temperature by cutting furnace power. The cooling rate from 2223 to 1773 K was estimated to be ca. 54 K/min. During the heating process, the sample was partially melted, and the densely sintered polycrystalline material was obtained. The sintered material was subsequently soaked in an aqueous solution of HCl (2 mol/L) at 298 K for 14 d for complete dissolution of the coexisting Al_4C_3 and Al_2OC compounds and Al(metal). The resulting porous granules were washed by distilled water and dried in an oven at 353 K for 8 h.

Inside the electric furnace, a small amount of O_2 gas that was adsorbed on the graphite insulation board would be continuously released during the heating process. In our previous studies on oxycarbides, we have confirmed that the experimental oxygen partial pressure (P_{O2}) in the furnace is necessarily kept near the carbon–carbon monoxide (CCO) buffer during the heating process.[12−15] Thus, the P_{O2}-value at 2223 K is estimated to be 1.6×10^{-14} atm (log P_{O2} = −13.80) based on the CCO buffer (Figure S2, see Supporting Information).[16,17] This implies that, at 2223 K and below, the Al_4C_3 component will be continuously oxidized by the reaction with CO gas during the heating and cooling process according to $Al_4C_3(s) + 6CO(g) \rightarrow 2Al_2O_3(s) + 9C(s)$.

Optical Microscopy and EPMA. One part of the granule sample was made into a thin section, and the microtexture was observed under an optical microscope. Quantitative spot analysis was made for the thin-section specimen using an electron probe microanalyzer (EPMA, JXA-8900L, JEOL Ltd., Tokyo, Japan). The correction for intensities was made using the ZAF routines. A sintered specimen of Al_4O_4C was used for the standard material.

X-ray Powder Diffraction. The other part of the sample was finely ground to obtain powder specimen and introduced into a glass capillary tube of internal diameter ca. 0.4 mm. The XRPD intensities were collected on a diffractometer (SmartLab, Rigaku Co., Tokyo, Japan), equipped with an incident-beam Ge(111) Johansson monochromator to obtain Cu $K\alpha_1$ radiation, and a high-speed detector (Rigaku D/teX) was used in the Debye–Scherrer geometry. The X-ray generator was operated at 45 kV and 200 mA. Other experimental conditions are given in Table 1. No preferred orientation could be seen in the diffraction pattern which was collected with the specimen rotating. We corrected the X-ray absorption using the μr value (μ, linear absorption coefficient; r, sample radius) of the sample and capillary tube, which was determined by the transmittance of direct incident beam. The entire experimental diffraction pattern was employed for the crystal-structure analysis. The structure data were standardized according to the rules formulated by Parthé and Gelato[18] using the computer program STRUCTURE TIDY.[19] The EDD with 64 × 64 × 614 pixels in the unit cell, the spatial resolution of which is approximately 0.005 nm, were obtained from the MPF method using the computer programs RIETAN-FP[20] and Dysnomia.[21] The crystal structure models and equidensity isosurfaces of EDD were visualized with the computer program VESTA.[22]

Table 1. Conditions of the XRPD Experiment and Parts of Data Related to the Rietveld Refinement for $Al_3O_{3.5}C_{0.5}$

chemical formula	$Al_3O_{3.5}C_{0.5}$
space group	$R\bar{3}m$ (No. 166)
a/nm	0.29588(1)
c/nm	2.84080(7)
V/nm^3	0.21538(1)
Z	3
D_x/Mg m^{-3}	3.306
wavelength/nm	0.154 0593 (Cu $K\alpha_1$)
2θ range/deg	5.0−157.0
step size, 2θ /deg	0.01
total experimental time/h	12.7
no. of intensity data	15 201
no. of contributing reflections	112
no. of refined structural parameters	63
no. of background parameters	12
no. of nonlinear constraints	24
R_{wp} (Rietveld)	0.041 10
S (Rietveld)	1.199
R_p (Rietveld)	0.031 37
R_B (Rietveld)	0.019 64
R_F (Rietveld)	0.014 31
R_B (MPF)	0.008 24
R_F (MPF)	0.007 19

Transmission Electron Microscopy. The powder specimen was also examined using TEM (JEM 2100F, JEOL ltd., Tokyo, Japan) operated at 200 kV and equipped with an electron energy loss spectrometer (EELS, Enfina, Gatan Inc., Pleasanton, CA). The powder particles were deposited with ethyl alcohol on a copper grid. Selected area electron diffraction (SAED) patterns and corresponding lattice images were obtained. The multislice simulation image, which was generated using a software package xHREM (HREM Research Inc., Saitama, Japan), was compared with the high resolution image to confirm the validity of the structural model.

RESULTS AND DISCUSSION

Microtextures and Chemical Compositions. The optical microscopic observation (Figure 1) indicated that the sample was composed mainly of lath-shaped transparent crystals, together with a smaller amount of opaque materials that were amorphous or poorly crystalline as evidenced by XRPD. The XRPD pattern also showed the coexistence of the trivial amount of α-Al_2O_3 (Figure 2). The analyzing spots for EPMA were selected carefully for the lath-shaped crystals under the microscope since most of the crystal grains were deficient in size. We found relatively large crystal grains up to 15 μm and determined the average chemical composition by measuring one point for each of the three crystal grains to be 43.3(4) mol % Al, 50.7(2) mol % O, and 6.0(5) mol % C, where the figures in parentheses indicate standard deviations. The anion ratios were derived on the basis of three Al atoms to be [Al:O:C] = [3:3.51(3):0.41(4)], indicating that the [Al:O:C] ratios are [3:3.5:0.5]. In the light of the chemical composition (87.5 mol

dx.doi.org/10.1021/ic302674g | Inorg. Chem. 2013, 52, 2648−2653

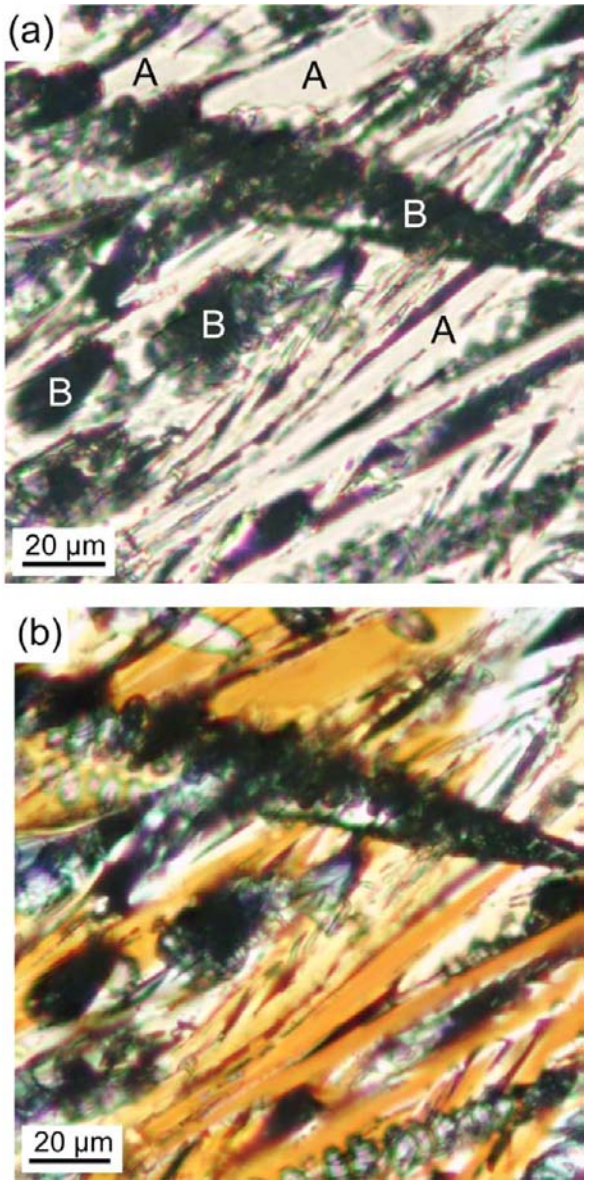

Figure 1. Optical micrographs showing the lath-shaped transparent crystals (labeled "A") and opaque materials (labeled "B"). Thin section. (a) Open polar and (b) crossed polars.

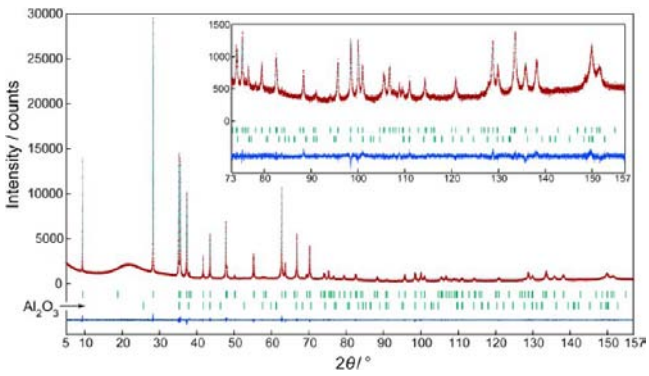

Figure 2. Comparison of the observed diffraction pattern of $Al_3O_{3.5}C_{0.5}$ and α-Al_2O_3 (symbol: +) with the corresponding calculated pattern (upper solid line). The difference curve is shown in the lower part of the diagram. Vertical bars indicate the positions of Bragg reflections.

% Al_2O_3 and 12.5 mol % Al_4C_3, see Figure S1 in Supporting Information), the relevant compound must be of the new material reported by Sitnikov et al.[2] The habit of the lath-shaped crystals would be responsible for the rapid crystallization of the melt during the cooling process.

The chemical compositions of the opaque materials were found to be rich in carbon content, the average composition of which was determined by measuring one point for each of nine grains to be 7.7(32) mol % Al, 16.6(70) mol % O, and 75.7(63) mol % C. The carbon component of the opaque materials could be provided by the oxidation reaction of Al_4C_3 component. We also determined the average chemical composition of the whole sample by examining 91 points randomly in the region of 2 mm squares on the thin section to be 39(11) mol % Al, 46(10) mol % O, and 14(21) mol % C. As a result, the average chemical composition of the starting mixture are in the Al–Al_2O_3–Al_4C_3 ternary region, while those of the whole sample and opaque materials are in the quadrilateral region of Al_2O_3–Al_4C_3–O–C (Figure S1, see Supporting Information).

Crystal Structure Determination from XRPD Data. The XRPD pattern showed the presence of relatively weak diffraction intensities peculiar to α-Al_2O_3[23] (Figure 2). All of the other diffraction peaks belonging to the lath-shaped crystals were successfully indexed with the hexagonal cell with dimensions of a = ca. 0.30 nm and c = ca. 2.84 nm. The individual integrated intensities and cell dimensions were refined by the Le Bail method[24] using the computer program RIETAN-FP.[20] The observed diffraction peaks were examined to confirm the presence or absence of reflections. Systematic absences $h - k + l \neq 3n$ for $hkil$ reflections were found, which implies that possible space groups are $R3$, $R\bar{3}$, $R32$, $R3m$, and $R\bar{3}m$. All of the possible space groups were tested by the powder charge-flipping method using the computer program Superflip[6,7] for crystal structure determination. Because the carbon concentration was relatively low, a unit-cell content of [9Al 12O] was used as input data for the search of an initial structure model. The promising structural models were successfully obtained for the space groups $R\bar{3}$, $R32$, and $R\bar{3}m$. We adopted the structural model with the last space group because of the highest symmetry. There are five independent sites in the unit cell; three Al sites at Wyckoff positions 3a (Al1) and 6c (Al2a and Al2b), and two O/C sites at 6c. Because of the unusually short distance (= ca. 0.11 nm) between Al2a and Al2b, these 6c sites (point symmetry 3m) can be regarded as the split sites of the same symmetry site of 6c.

The refinement (see Supporting Information) resulted in the satisfactory reliability (R) indices[25] (Table 1), indicating that the disordered arrangement of Al2 site can be represented adequately with the split-atom model in Figure 3a. The positional and isotropic atomic displacement (U) parameters of atoms are given in Table 2. It should be noted that the site occupancies are nearly equal to $^3/_4$ for Al2a and $^1/_4$ for Al2b. Quantitative X-ray analysis with correction for microabsorption according to Brindley's procedure[26] was implemented in the program RIETAN-FP. The crystalline phase composition of the sample was found to be 97.9 mol % $Al_3O_{3.5}C_{0.5}$ and 2.1 mol % α-Al_2O_3, on the assumption that both effective particle radii of the two phases were 5.00 μm.

The MPF method was subsequently used to confirm the validity of the split-atom model. After three REMEDY cycles, the subtle EDD changes as revealed by MPF significantly improved the R_B and R_F indices (Table 1). The decreases in R indices demonstrate that the present disordered structure can

dx.doi.org/10.1021/ic302674g | Inorg. Chem. 2013, 52, 2648–2653

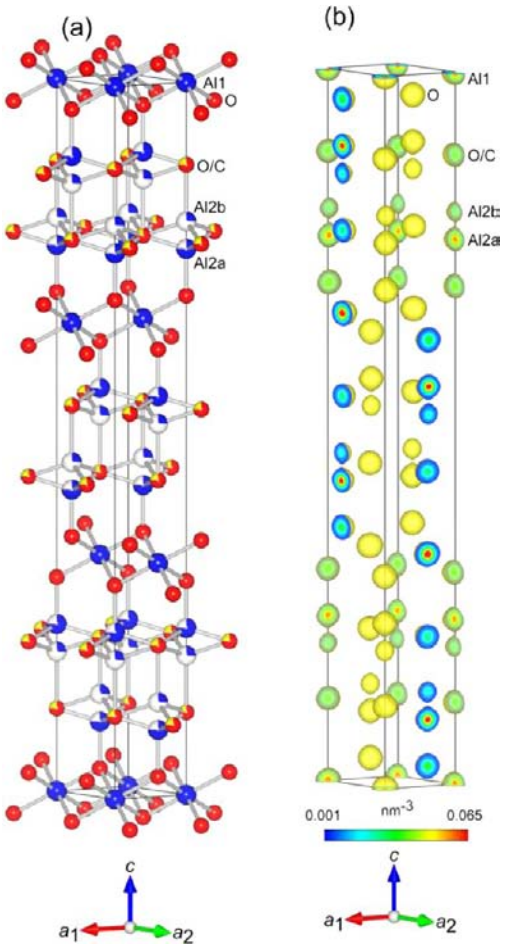

Figure 3. (a) Crystal structure of $Al_3O_{3.5}C_{0.5}$ (space group $R\bar{3}m$) and (b) three-dimensional electron density distribution determined by MPF. All the atoms in part a are expressed as solid spheres. Because the occupancies of Al2a and Al2b sites are less than unity, the Al atoms occupying there are displayed as blue circle graphs for occupancies. Red and yellow bicolor balls are for oxygen (red) and carbon (yellow) sites. Isosurfaces in part b expressed in smooth shading style for an equidensity level of 0.001 nm^{-3}. Atom numbering in parts a and b corresponds to that given in Table 1.

Table 2. Structural Parameters and Atomic Displacement Parameters ($\times 10^{-2}$ nm^2) for $Al_3O_{3.5}C_{0.5}$

site	Wyckoff position	*g*	*x*	*y*	*z*	*U*
Al1	3*a*	1	0	0	0	0.0094(2)
Al2a	6*c*	0.745(1)	0	0	0.23391(2)	0.0071(2)
Al2b	6*c*	0.255	0	0	0.19499(7)	0.0071
O/C	6*c*	0.75/0.25	0	0	0.11634(4)	0.0139(2)
O	6*c*	1	0	0	0.29981(3)	0.0089(3)

be seen more clearly from EDD rather than from the conventional structural parameters reported in Table 2. Observed, calculated, and difference XRPD patterns for the MPF are plotted in Figure 2. The EDD determined by MPF are in reasonably good agreement with the atom arrangements (Figure 3b). We therefore concluded that, as long as the crystal structure was expressed by a ball-and-stick structural model, the present split-atom model would be satisfactory.

Structure Description. The coordination elements of the structure are $[AlO_6]$ octahedron and two types of $[Al(O,C)_4]$ tetrahedra. The ionic radii of Al^{3+} in the 6-fold coordination [$r(Al^{3+}(6))$ = 0.0535 nm and $r(O^{2-}(4))$ = 0.138 nm][5] predicts the interatomic distance of 0.1915 nm for Al−O. This predicted value is in good agreement with the Al−O distance of 0.1956 nm in $[Al1O_6]$ octahedron (Table S1, see Supporting Information). The average interatomic distances are longer for the $[Al2b(O,C)_4]$ tetrahedron (0.192 nm) than for the $[Al2a(O,C)_4]$ tetrahedron (0.180 nm). This difference in interatomic distance is probably caused by the higher concentration of C for the former tetrahedral ligand (25% C and 75% O) than for the latter ligand (18.75% C and 81.25% O) since the average interatomic distance would increase with increasing C/(C + O) ratio as evidenced by the two extremes of $[AlC_4]$ and $[AlO_4]$ tetrahedra.

The crystal structure of $Al_3O_{3.5}C_{0.5}$ can be regarded as intergrowth structure, which consists of the α-Al_2O_3-type $[AlO_2]$ single layers (denoted by A) with thickness of ca. 0.191 nm separated by the $[Al_2(O,C)_4]$ unit layers (B) of ca. 0.756 nm thickness (Figure 3a). The atom arrangement of the former layer is similar to that of α-Al_2O_3 because, between the two oxygen layers, there are positions for Al atoms such that each ones is octahedrally surrounded by six O atoms. Although one-third of the available positions are vacant for α-Al_2O_3, all of those are filled for the present $[AlO_2]$ layer. The atom arrangement of the $[Al_2(O,C)_4]$ unit layer can be described in terms of a three-dimensional network of $[Al(O,C)_4]$ tetrahedra which are associated by sharing corners. These two types of layers are alternately stacked in the *c*-axis direction with a sequence ⟨ABABAB⟩ in the unit cell to form a three-dimensional structure.

Antiphase-Domain Structure. We have confirmed using EELS that the lath-shaped crystals are composed of a small amount of C atoms together with O atoms (Figure 4). The

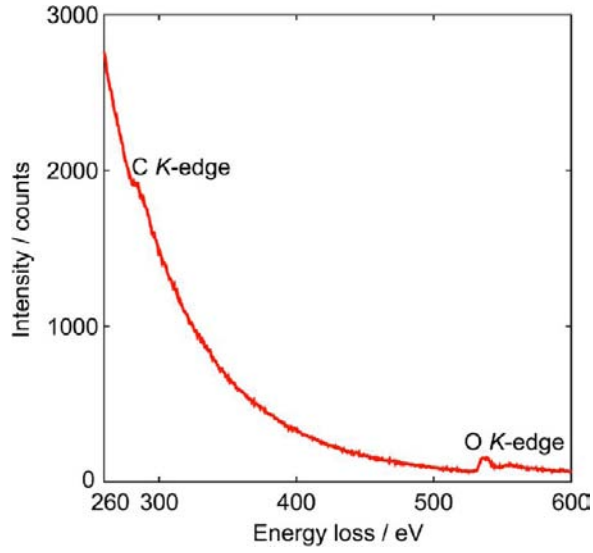

Figure 4. Identification of the presence of C and O in the compound. Electron energy loss spectrum.

main diffraction spots of SAED pattern in Figure 5a, obtained from the selected area of ca. 500 nm in diameter, were successfully indexed with the hexagonal cell with dimensions of *a* = ca. 0.30 nm and *c* = ca. 2.84 nm. The corresponding lattice image (Figure 5b) strongly suggests that the crystal is characterized by a layered structure with the periodicity of ca. 2.8 nm along the *c* axis. The intensity distribution of the main

dx.doi.org/10.1021/ic302674g | Inorg. Chem. 2013, 52, 2648−2653

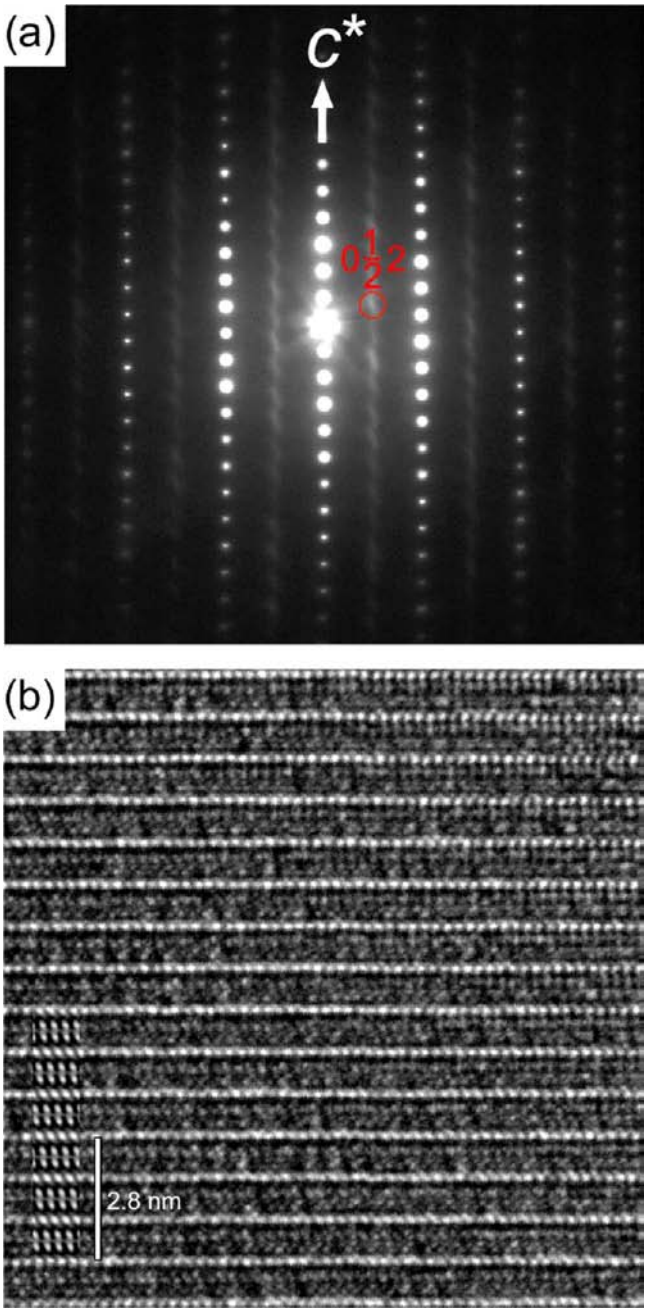

Figure 5. (a) Selected-area electron diffraction pattern and (b) corresponding lattice image. Incident beam almost parallel to the hexagonal *a* axis. The red open circle in part a indicates the superstructure reflection with the indices $0\ ^1/_2\ 2$. The simulated image of $Al_3O_{3.5}C_{0.5}$ (specimen thickness = 88.8 nm and defocus value = −400 nm) is inserted in the lattice image in part b.

spots and the lattice image are consistent with the present structural model determined by XRPD; the distributions of black and white contrast of the simulated image were consistent with those of the corresponding high resolution micrograph.

However, all of the diffraction spots including very weak ones (Figure 5a) lead to a doubling of the *a* axis with respect to the hexagonal basic cell. Actually, we have observed APDs using dark-field TEM technique (Figure 6). Since the superstructure reflections as recognized in the SAED pattern have never been detectable for the XRPD pattern, the dimensions of the APDs must be within the coherence range of X-rays. As shown in

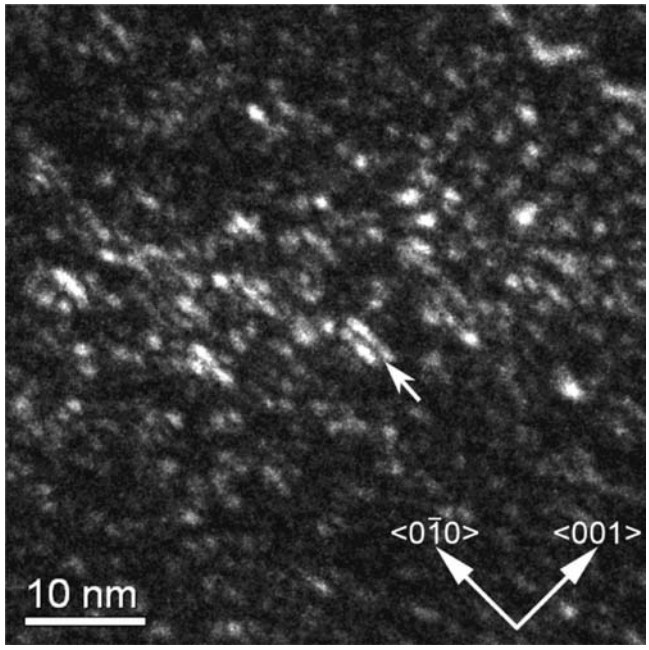

Figure 6. Dark-field image formed with the $0\ ^1/_2\ 2$ reflection, showing APD boundaries. One of the distinct boundaries is indicated by an arrow.

Figure 6, the size distribution of the APDs ranges from 1 to 2 nm along the *c* axis and from 2 to 4 nm for the direction perpendicular to the *c* axis for this compound.

The most plausible explanation for the formation of APDs in $Al_3O_{3.5}C_{0.5}$ is that the phase transition from the high-temperature (H) phase to the low-temperature (L) phase, which must be accompanied by the loss of translational symmetry, occurs on cooling. The size of the unit cell would be increased by 4 during the phase transition since the unit-cell dimensions of the H-phase (a_H and c_H) and those of the L-phase (a_L and c_L) would be related by $a_L \approx 2 \times a_H$ and $c_L \approx c_H$. The number of variants possible to produce during the phase transition is 4. These four variants are related across the antiphase boundaries by the displacement vectors $1/2[100]_L$, $1/2[010]_L$, and $1/2[110]_L$. We have observed the APDs that are related by the displacement vector $1/2[010]$ (Figure 6). The displacement vectors in the H-phase can acquire different energies in the L-phase. Thus these energy difference can favor the formation of one orientation over the other.

Structural Models Proposed for the H- and L-Phases. We have constructed one of the probable atom arrangements in the antiphase domains, taking into consideration of the site occupancies of Al atoms in the crystal structure ([*g*(Al2a):*g*(Al2b)] = [3:1]). There are eight independent sites in the *ordered* structural model (space group $R\bar{3}m$ and $Z = 12$): four Al sites at Wyckoff positions 3*a* (Al1), 6*c* (Al2), 9*e* (Al3), and 18*h* (Al4); two O/C sites at 6*c* and 18*h*; and two O sites at 6*c* and 18*h* (Table S2, see Supporting Information). Each of the Al1 and Al3 atoms is coordinated by six O atoms. The Al4 and Al2 sites, corresponding to the former Al2a and Al2b sites, respectively, are coordinated by four (O, C) atoms (Figure S3, see Supporting Information). The numbers of these sites in the unit cell (*N*) are 18 for Al4 and 6 for Al2 ($[N_{Al4}:N_{Al2}] = [3:1]$). The crystal structure is characterized by the two types of tunnel-like cavities running parallel to ⟨100⟩ (Figure S4, see Supporting Information). With the H-phase, one of the most

dx.doi.org/10.1021/ic302674g | *Inorg. Chem.* 2013, 52, 2648−2653

plausible structural models would be obtained by unifying the split sites (Al2a and Al2b) into a single Al site, the z-coordinate of which would be close to 0.215 ($\approx\{z(\mathrm{Al2a}) + z(\mathrm{Al2b})\}/2$).

CONCLUSION

We have determined the electron density distributions and crystal structure of $Al_3O_{3.5}C_{0.5}$ in the Al_2O_3−Al_4C_3 system. The crystal structure was satisfactorily represented by the split-atom model with the space group $R\bar{3}m$ (centrosymmetric). The MPF method was used to confirm the validity of the structural model. The three-dimensional EDD determined by MPF were in reasonably good agreement with the atom arrangements. The dark-field TEM showed that the crystal was composed of APDs related by the unit-lattice translation, suggesting the occurrence of the high−low phase transition. Thus, the present structural model determined by the X-ray diffraction method might be of the average crystal structure of the low-temperature phase.

ASSOCIATED CONTENT

Supporting Information

CIF dataa, tables (interatomic distances and structural parameters), and figures (chemical compositions, phase boundaries and ordered structural model). This material is available free of charge via the Internet at http://pubs.acs.org.

AUTHOR INFORMATION

Corresponding Author

*E-mail: fukuda.koichiro@nitech.ac.jp.

Notes

The authors declare no competing financial interest.

ACKNOWLEDGMENTS

Thanks are due to Drs. T. Iwata and H. Toraya, Rigaku Co. Japan, for their technical assistance in XRPD.

REFERENCES

(1) Qui, C.; Metselaar, R. Z. *Metallkd.* **1995**, *86*, 198.
(2) Sitnikov, P. A.; Lopatin, S. I.; Ryabkov, Yu. I.; GrassJuly, V. E. *Russ. J. Gen. Chem.* **2004**, *74*, 989.
(3) Bragg, L.; Claringbull, G. F. In *Crystal Structures of Minerals*; G. Bell and Sons Ltd.: London, 1965.
(4) Th. Gesing, M.; Jeitschko, W. *Z. Naturforsch.* **1995**, *50b*, 196.
(5) Shannon, R. D. *Acta Crystallogr.* **1976**, *A32*, 751.
(6) Oszlanyi, G.; Suto, A. *Acta Crystallogr.* **2004**, *A60*, 134.
(7) Palatinus, L.; Chapuis, G. *J. Appl. Crystallogr.* **2007**, *40*, 786.
(8) Rietveld, H. M. *Acta Crystallogr.* **1967**, *22*, 151.
(9) Takata, M.; Nishibori, E.; Sakata, M. *Z. Kristallogr.* **2001**, *216*, 71.
(10) Izumi, F. *Solid State Ionics* **2004**, *172*, 1.
(11) Nord, G. L., Jr. In *Minerals and Reactions at the Atomic Scale: Transmission Electron Microscopy: Imaging Transformation-Induced Microstructures*; Buseck, P. R., Ed.; Mineralogical Society of America: Washington, DC, 1992; pp 455−508.
(12) Kaga, M.; Urushihara, D.; Iwata, T.; Sugiura, K.; Nakano, H.; Fukuda, K. *J. Solid State Chem.* **2010**, *183*, 2183.
(13) Inuzuka, H.; Kaga, M.; Urushihara, D.; Nakano, H.; Asaka, T.; Fukuda, K. *J. Solid State Chem.* **2010**, *183*, 2570.
(14) Urushihara, D.; Kaga, M.; Asaka, T.; Nakano, H.; Fukuda, K. *J. Solid State Chem.* **2011**, *184*, 2278.
(15) Urushihara, D.; Asaka, T.; Takeda, T.; Hirosaki, N.; Fukuda, K. *Powder Diffr.* **2011**, *26*, 4.
(16) Kulikov, I. S. *Thermodynamics of Oxides*, Metallurgiya: Moscow, 1986.
(17) *NIST-JANAF Thermochemical Tables*, 4th ed.; Chase, M. W., Jr., Ed.; Journal of Physical Chemistry Reference Data Monograph No. 9; American Chemical Society and American Institute of Physics: Woodbury, NY, 1998.
(18) Parthé, E.; Gelato, L. M. *Acta Crystallogr.* **1984**, *A40*, 169.
(19) Gelato, L. M.; Parthé, E. *J. Appl. Crystallogr.* **1987**, *20*, 139.
(20) Izumi, F.; Momma, K. *Solid State Phenom.* **2007**, *130*, 15.
(21) Izumi, F.; Momma, K. *IOP Conf. Ser.: Mater. Sci. Eng.* **2011**, *18*, 022001.
(22) Momma, K.; Izumi, F. *J. Appl. Crystallogr.* **2011**, *44*, 1272.
(23) Lutterotti, L.; Scardi, P. *J. Appl. Crystallogr.* **1990**, *23*, 246.
(24) Le Bail, A.; Duroy, H.; Fourquet, J. L. *Mater. Res. Bull.* **1988**, *23*, 447.
(25) Young, R. A. Introduction to the Rietveld Method. In *The Rietveld Method*; Young, R. A., Ed.; Oxford University Press: Oxford, U.K., 1993; pp 1−38.
(26) Brindley, G. W. *Bull. Soc. Chim. Fr.* **1949**, D59.